Applied Acoustics 99 (2015) 118–124

Contents lists available at ScienceDirect

Applied Acoustics

journal homepage: www.elsevier.com/locate/apacoust

Transfer function of small convergent–divergent (C–D) nozzles and opposite (D–C) devices filled with thermo-viscous fluid at rest

Petr Honzík [a,c,*], François Fohr [b], Michel Bruneau [a]

[a] Laboratoire d'Acoustique de l'Université du Maine, UMR CNRS 6613, Université du Maine, Avenue Olivier Messiaen, 72 085 Le Mans, France
[b] Centre de Transfert de Technologie du Mans, Département Acoustique, 20 rue Thalès de Milet, 72 000 Le Mans, France
[c] Czech Technical University in Prague, Faculty of Transportation Sciences, Konviktská 20, 110 00 Praha 1, Czech Republic

ARTICLE INFO

Article history:
Received 4 October 2014
Received in revised form 28 May 2015
Accepted 1 June 2015
Available online 19 June 2015

Keywords:
Acoustic transfer function
Convergent–divergent devices
Thermo-viscous fluid

ABSTRACT

An analytical representation, which involves single integrals, is established for describing the shape of small acoustic elements (slits or tubes) more or less tapered (the shape being governed by only one parameter). This representation includes the ability to create a zero slope (horizontal) at one end and an infinite one (vertical) at the other end, the limiting shapes being small cylindrical tubes or cavities. Then, the results obtained from the analytic procedure presented in a previous paper (Honzík et al., 2013), whereby one expresses the transfer function of such elements filled with a thermo-viscous fluid and, beyond, the transfer function of components obtained when connecting them continuously, are presented and compared to numerical and experimental results. Two prototype components gradually narrowing and widening, and conversely, are considered, namely a convergent–divergent nozzle which makes a symmetric hourglass-shape and the opposite divergent–convergent device, with different loads that end the device. The results show the potentialities of such small components when used in acoustic devices.

1. Introduction

In recent years, much efforts has been put into miniaturizing acoustic elements (such as tubes, slits, and cavities) used in acoustic devices (typically small filters), in order to reduce the sizes of these devices and to lower their manufacturing cost (MEMS devices are more particularly concerned). Most of the analytical and numerical works on the behavior of the acoustic devices which are made up of these elements deal primarily with (i) the description of input impedances or transfer functions which account for the coupling between elements (most often through the behavior of adapted lumped element circuits), (ii) the modeling of the dissipative effects of tubes and slits, (iii) the modeling of the effect of both the inertia of fluid in small guides and the stiffness of fluid in cavities [1–12]. In these devices, the dissipation can be controlled by the transverses dimensions of the slits or the tubes, and the resonances can be controlled by the volume of the cavities, both being also controlled by the lengths of the slit or the tubes.

Although these small scale devices have been extensively studied because they are of practical interest today, the profiles of the input impedances or transfer functions, as functions of the frequency, especially when resonances occur, are always difficult to handle when dissipation and resonance frequencies are settled. One route to handle these shapes is the use of tapered tubes, slits and cavities, instead of the non-tapered elements mentioned above. Being concerned by such tapered elements, an accurate method (among others) to solve approximately the one-dimensional analytical problem has been published recently (see [11] and references contained therein): it relies on representation which enables analytical estimates in the long wavelength range, through a global transfer matrix for each element, using the formal solution provided by the Volterra integral equation.

In order to be able both to create analytically a quite vast range of shapes of varying cross-sectional area of the acoustic elements, including the ability to create a zero slope (horizontal) at one end and an infinite one (vertical) at the other end, and to associate continuously theses elements (avoiding gaps of the shape and of the slope between successive elements), a specific formulation is used here. This formulation relies on an integral representation of both the axial coordinate and the radius (or the thickness) of the element considered. This formulation depends on only one more parameter than for the classical non tapered elements, namely

* Corresponding author at: Czech Technical University in Prague, Faculty of Transportation Sciences, Konviktská 20, 110 00 Praha 1, Czech Republic.
E-mail addresses: Petr.Honzik@gmail.com (P. Honzík), ffohr@cttm-lemans.com (F. Fohr), Michel.Bruneau@univ-lemans.fr (M. Bruneau).

http://dx.doi.org/10.1016/j.apacoust.2015.06.001
0003-682X/

the slope of the radius or of the thickness at one end for a given length of the element, the other parameters being approximately fixed as mentioned above by dissipation and resonance frequencies looked for.

The analytical procedure which leads to describe the geometry of the tapered tubes considered herein, involving single integrals, is proposed in the next section. Then in the following section, the procedure to obtain the transfer matrix of each tapered element and of the whole component made up of such connected elements, filled with thermo-viscous fluid, is given from using the analytical model presented previously in the literature [11]. Numerical and experimental results are presented and compared to the analytical ones, for these components made up of tubes tapered (gradually narrowing or widening) or not. Two prototype components are considered, a convergent–divergent nozzle making a symmetric hourglass-shape and the opposite divergent–convergent device, both made by taking two copies of a shape wide at one end that narrows to the other end and connecting them symmetrically by the narrow end and the wide end respectively (Fig. 4). The results obtained show the potentialities of such small components, with different loads that end them.

2. Formulation used to describe shapes of tapered axisymmetric acoustic elements

The structures considered below are two dimensional axisymmetric tapered tubes (tapered slits can be treated in the same manner). The basic profile in the plane (u, v) shown in Fig. 1, from which the analytical shapes of the tapered tubes considered below are expressed, is represented by a curve starting from the coordinate $(u = 0, v = 0)$ with a vanishing slope, the normalized curvilinear coordinate along the curve being denoted w $[w \in (0, 1)]$. At the end of the curve $(w = 1)$, the angle θ of the tangent of the curve with the u-axis is given by $\theta = \theta_0$. It is noteworthy that herein $\theta < \theta_0 < \pi/2$, the value $\theta_0 = 0$ corresponding to a cylindrical tube and $\theta_0 = \pi/2$ to a tapered tube with an infinite slope at its end (which is important in the present modeling). The analytical procedure whereby one expresses the shape of such curves could rely on the following expressions, α being a free parameter:

$$\begin{cases} u(w) = \int_0^w \cos(\theta_0 t^\alpha)\mathrm{d}t, \\ v(w) = \int_0^w \sin(\theta_0 t^\alpha)\mathrm{d}t. \end{cases} \tag{1}$$

These expressions give the following expected properties:

$$\begin{cases} (\mathrm{d}u)^2 + (\mathrm{d}v)^2 = (\mathrm{d}w)^2, \\ \tan(\theta) = \mathrm{d}v/\mathrm{d}u = \tan(\theta_0 t^\alpha) \Rightarrow \theta = w^\alpha \theta_0. \end{cases} \tag{2}$$

Note that this representation has been inspired by the well-known curve called clothoid or Cornu's spiral, which corresponds to $\alpha = 2$.

For the two dimensional axisymmetric tapered tubes considered below, the axial coordinate is denoted x, the radial coordinate R, and the angle of the tangent of the curve with the x-axis is denoted β. At the ends of the curve, respectively $w = 0$ and $w = 1$ for configurations (a) and (b) or reversely for configurations (c) and (d) (see below), the coordinate x is given by $x = -L$ respectively $x = 0$, the coordinate r is given by $R(-L)$ respectively $R(0)$ with $|R(-L) - R(0)| = H$, and the angle β is either vanishing or denoted β_0. Starting from the approach given above (Eqs. (1) and (2)), different kinds of tapered tubes can be modeled in the plane (R, x), depending on the change of variables chosen. The four cases which are useful are presented in Fig. 2. They correspond respectively to the following relationships, where U, V, and E are defined as

$$U = u(1) = \int_0^1 \cos(\theta_0 t^\alpha)\mathrm{d}t,$$
$$V = v(1) = \int_0^1 \sin(\theta_0 t^\alpha)\mathrm{d}t, \quad E = \frac{U}{L}\frac{H}{V}: \tag{3}$$

(a) divergent tube with horizontal slope on the left $x = -L$ (Fig. 2a)

$$x = (u - U)L/U, \quad R(x) = R(-L) + vH/V,$$
$$\tan(\beta) = E\tan(\theta_0 w^\alpha), \tag{4}$$

(b) convergent tube with horizontal slope on the left $x = -L$ (Fig. 2b)

$$x = (u - U)L/U, \quad R(x) = R(-L) - vH/V,$$
$$\tan(\beta) = -E\tan(\theta_0 w^\alpha), \tag{5}$$

(c) tube with horizontal slope on the right $x = 0$ (widest end) (Fig. 2c)

$$x = -uL/U, \quad R(x) = R(0) - vH/V, \quad \tan(\beta) = E\tan(\theta_0 w^\alpha), \tag{6}$$

(d) tube with horizontal slope on the right $x = 0$ (narrowest end) (Fig. 2d)

$$x = -uL/U, \quad R(x) = R(0) + vH/V, \quad \tan(\beta) = -E\tan(\theta_0 w^\alpha). \tag{7}$$

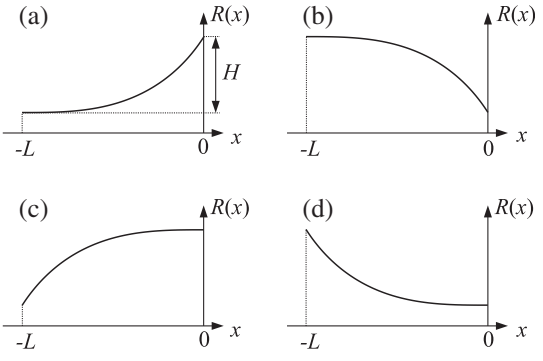

Fig. 2. Different kind of tapered tubes which can be modeled in the plane (R, x).

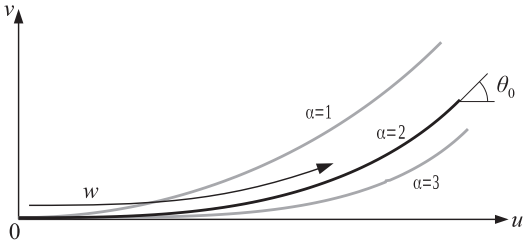

Fig. 1. Basic profile in the plane (u, v) from which the analytical shapes of the tapered tubes are expressed.

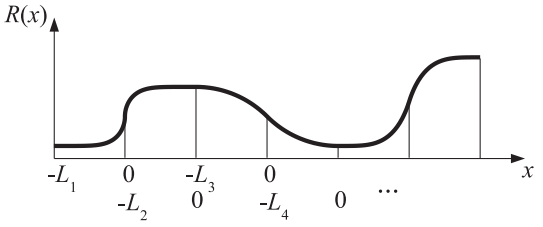

Fig. 3. Example of device involving several configurations of tapered tubes.

An example of device which can be made up of several configurations of tapered tubes is presented in Fig. 3, for given values of the parameters θ_0 and α, showing that the notations on the x-axis are defined for each tapered element. Note that a quite vast range of shapes can be created (even those having a horizontal slope at one end and vertical one at the other end).

3. Analytical results and comparison with numerical and experimental results

The remaining of the paper presents: (i) the analytical results obtained from using a method which provides a global transfer matrix for each tapered tube whose elements are given either in classical textbooks (cylindrical tubes) [3] or in a previous paper (tapered tubes) [11], (ii) comparisons with results obtained from numerical implementation which relies on a 2-D axisymmetrical simulations using an adaptive mesh and accounting for the viscous and thermal boundary layer effects [13], (iii) comparisons with experimental results obtained from a classical experimental set-up.

3.1. Analytical and numerical results

The analytical methodology used in a previous paper [11], mentioned above, to solve the 1-D propagation equation (see appendix Eq. (A.1)) for each tapered tube, which accounts for the effects of the viscous and thermal boundary layers, relies on an adapted change of variable to remove the first order spatial derivative, then on the associated Volterra integral equation, and finally on a perturbation method (for wavelengths much greater than the length of the components), in the frame of a transfer matrix method (see Appendix).

Therefore, the acoustic behavior of the component is described in each part (each element) by a transfer matrix (two successive parts being separated by the change of curvature or by the maximum or minimum of the curve given by the longitudinal cut of the component), leading to a global transfer matrix for the component as a whole then to the results of interest (pressure transfer function or input impedance). Note that the geometrical discontinuities between narrow tubes and cavities, when they exist, are accounted for by introducing in the formalism the usual equivalent, additional mass [3].

The numerical implementation (FEM) handled herein, against which the approximate analytical results can be tested, relies on 2-D axisymmetrical simulation using an adaptive mesh and accounting for the viscous and thermal boundary layer effects [13]. The linear formulation used to perform the numerical modeling is based upon two coupled equations involving the particle velocity $\mathbf{v}$ and the temperature variation τ (the acoustic pressure p being expressed in terms of these two variables) [14]. These two variables are subject to Dirichlet conditions on the rigid isothermal boundaries ($\mathbf{v} = \mathbf{0}$, $\tau = 0$). A time-periodic source set at the entrance is a virtual adiabatic ($\partial_n \tau = 0$) source described by its normal velocity [11,13,15]. This velocity is non-uniformly distributed over the section of the component: it has the same profile as the analytically calculated particle velocity (which accounts for the viscous boundary layers) over the diameter of the tube (which is the same as the one of the component entrance). Note that such profile of the input particle velocity vanishes at the wall of the component in order to avoid discontinuities of the particle velocity on the rigid boundaries that must satisfy the non-slip condition [11,15]. The results for the pressure transfer function and input impedance obtained from the numerical model have been calculated using mean quantities over cross-section at the input or output of the component.

In the examples chosen hereafter the component is either a convergent–divergent nozzle making a symmetric hourglass-shape or the opposite divergent–convergent component. The loads that end the component considered are of different natures: closed cavity or isothermal rigid wall. The analytical and numerical results are then calculated using the physical parameters of the thermo-viscous fluid (air in this case) given in Table 1.

Two classes of components considered below are shown in Fig. 4. They have a lower value (0.5 mm) and an upper value (3 mm) of the radius, a given total length (12 mm), and two values of the parameter α ($\alpha = 0.5$ and $\alpha = 10$), the associated rectangular shape ($\alpha \to \infty$) being given. For each value of the parameter α, Fig. 4a represents a convergent–divergent nozzle making a symmetric hourglass-shape and Fig. 4b represents the opposite divergent–convergent component. Both these components can be made by taking two copies of a shape wide at one end that narrows to the other end and connecting them symmetrically by the narrow end and the wide end respectively (see photographs in Fig. 10 in the Section 3.2).

The theoretical results for the divergent–convergent component (Fig. 4b) for three configurations (two values of the parameter α: $\alpha = 0.5$ and $\alpha = 10$ and the associated rectangular shape)

Table 1
Parameters of the thermo-viscous fluid [15].

Parameter	Value	Unit
Static pressure P_0	101325	Pa
Static temperature T_0	296.15	K
Relative humidity RH	50	%
Density ρ_0	1.180	kg m^{-3}
Adiabatic speed of sound c_0	345.9	m s^{-1}
Shear dynamic viscosity μ	1.830×10^{-5}	Pa s
Bulk dynamic viscosity η	1.098×10^{-5}	Pa s
Thermal conductivity λ_h	24.40×10^{-3}	W m^{-1} K^{-1}
Ratio of specific heats γ	1.400	–
Specific heat coefficient at constant pressure per unit of mass C_P	1.010×10^{3}	J kg^{-1} K^{-1}

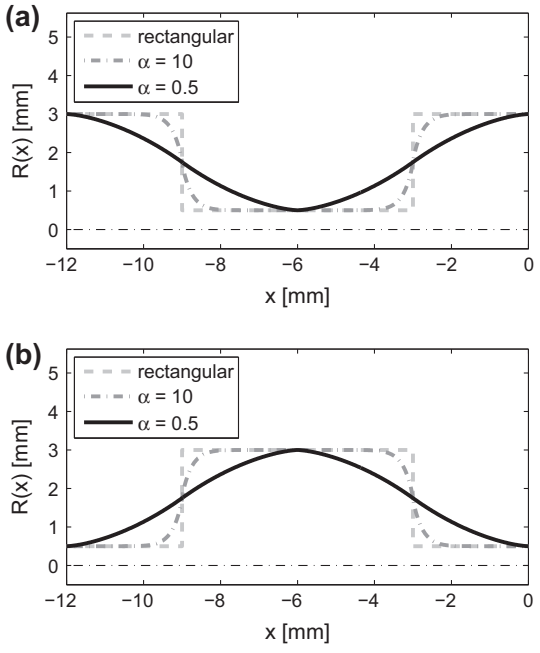

Fig. 4. (a) Convergent–divergent components and (b) divergent–convergent components whose shape depends on the value of the parameter α.

loaded by a rigid walled cylindrical cavity, radius 4 mm and depth 4 mm, are shown first. Fig. 5a and b show respectively the amplitudes (dB) and phases (rad) of the pressure transfer function between the input of the component and the bottom (the end) of the cavity, both as function of the frequency (logarithmic scale) respectively in the interval (100 Hz, 7 kHz). In each figure (and for all theoretical results presented below) the dashed line, the dashed-dotted line, and the full line represent the analytical results, respectively for the rectangular component, for $\alpha = 10$, and for $\alpha = 0.5$, and the dots, the crosses '+' and '×' marks represent the numerical values for the same shapes respectively. Generally, good agreement between the analytical and numerical results is observed (maximal difference at 1st resonance is 1.9 dB for $\alpha = 10$ and 0.8 dB for $\alpha = 0.5$, see the end of Section 3.2 for explanation about the discrepancies between analytical and numerical results). The curves show clearly that the value of the parameter α could have a decisive influence: without modifying significantly the Q-factor ($Q \in \{7, 12\}$) and the amplitude of the resonances ($\max|TF| \in \{18\text{ dB}, 23\text{ dB}\}$), the resonant frequency can be importantly translated (here for Example 670 Hz in the frequency range 1080–1750 Hz).

The convergent–divergent nozzle (Fig. 4a) considered below for three configurations ($\alpha = 0.5$ and $\alpha = 10$, and the associated rectangular shape), is the opposite of the divergent–convergent component considered above (with the same dimensions). The load that ends the component is an isothermal rigid wall. Fig. 6a and b show respectively the amplitudes (dB) and phases (rad) of the pressure transfer function between the input and the end of the component, both as function of the frequency (logarithmic scale) in the interval (100 Hz, 7 kHz). Good agreement between analytical and numerical results can be observed, the maximal difference at 1st resonance is 3 dB for $\alpha = 10$ and 3.8 dB for $\alpha = 0.5$, both being caused by a small shift in resonant frequency. Once more, these curves show clearly that the value of the parameter α could have a decisive influence: without modifying significantly the Q-factor ($Q \in \{9, 16\}$) and the amplitude of the resonances ($\max|TF| \in \{19\text{ dB}, 24\text{ dB}\}$), the resonant frequency can be importantly translated (here 1600 Hz in the frequency range 1900–3500 Hz).

In practical applications some uncertainties of geometrical parameters, including the parameter α, occur. Table 2 shows that the impact of the small change of α (±1% and ±5%) on the variation of the maximum of the transfer function (1st resonance) and of the Q-factor for D–C and C–D components is small for given dimensions.

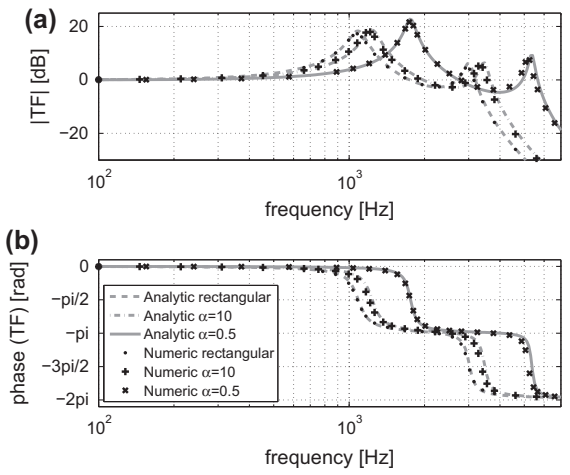

Fig. 5. (a) Amplitude (dB) and (b) phase (rad) of the pressure transfer function of the D–C component, both as function of the frequency (logarithmic scale) respectively in the interval (100 Hz, 7 kHz).

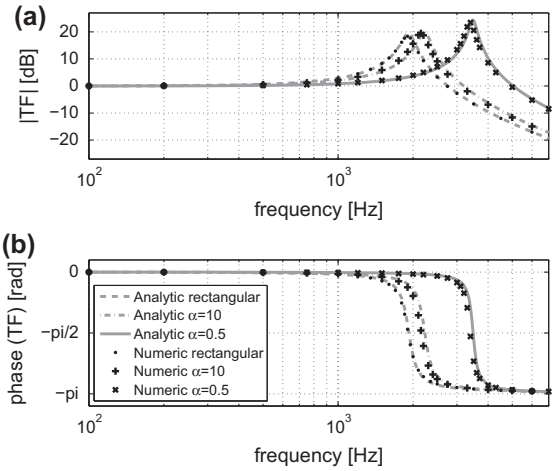

Fig. 6. (a) Amplitude (dB) and (b) phase (rad) of the pressure transfer function of the C–D component, both as function of the frequency (logarithmic scale) respectively in the interval (100 Hz, 7 kHz).

Table 2
Impact of small variations of the parameter α on the maximum of the transfer function and the Q-factor.

	Variation of α	Var. of max(|TF|)		Var. of Q-factor	
α		D–C	C–D	D–C	C–D
0.5	+1%	−0.014 dB	−0.016 dB	−0.19%	−0.18%
	−1%	+0.014 dB	+0.016 dB	+0.16%	+0.17%
	+5%	−0.069 dB	−0.077 dB	−0.83%	−0.84%
	−5%	+0.071 dB	+0.079 dB	+0.85%	+0.87%
10	+1%	−0.007 dB	−0.008 dB	−0.11%	−0.08%
	−1%	+0.007 dB	+0.007 dB	+0.10%	+0.10%
	+5%	−0.033 dB	−0.036 dB	−0.41%	−0.43%
	−5%	+0.037 dB	+0.039 dB	+0.46%	+0.46%

Fig. 7 shows the shapes of the divergent–convergent resonator considered here for three configurations: two values of the parameter α ($\alpha = 0.5$ and $\alpha = 10$) and the associated rectangular shape. The lower and upper values of the radius are respectively equal to 0.5 mm and 3 mm, and the lengths of the two parts of the component are respectively equal to 3 mm and 6 mm (total length being 9 mm). The load that ends the component is an isothermal rigid wall. This time the input impedance as function of the frequency (logarithmic scale) is shown in Fig. 8. Once more, as expected, these curves show clearly that the influence of the value of the parameter α could have a decisive influence: without

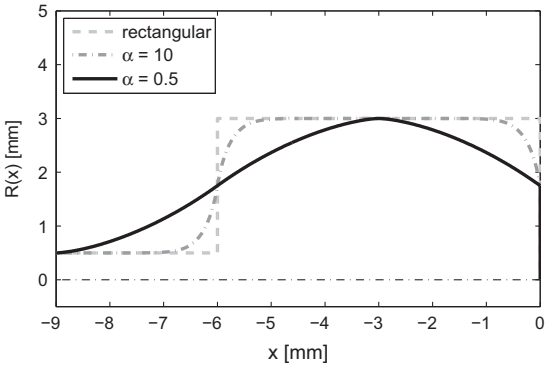

Fig. 7. Divergent–convergent resonators with several shapes and an isothermal rigid wall at the end.

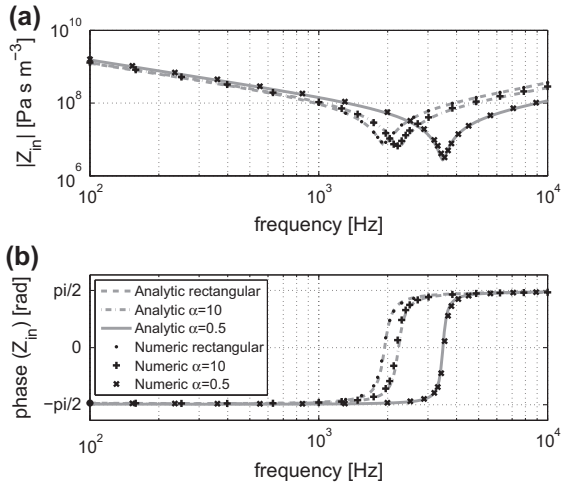

Fig. 8. (a) Modulus (Pa s m^{-3}) and (b) phase (rad) of the input impedance of the D–C resonator, both as function of the frequency (logarithmic scale) respectively in the interval (100 Hz, 10 kHz).

modifying drastically the depth of the minimum of the amplitude ($\min|Z_{in}| \in \{2.7 \times 10^6$ Pa s m^{-3}, 7×10^6 Pa s m^{-3}) and the shape of the curve, the resonant frequencies can be importantly translated (here 1500 Hz in the frequency range 2000–3500 Hz). Note that, in terms of lumped equivalent circuit associated with this resonator, the dissipative and inertial effects are lowered while the stiffness is enhanced when $\alpha = 0.5$ (compared with the other values of α presented), which leads to a higher resonant frequency.

3.2. Experimental results

The experimental results given below have been measured using the measurement set-up presented in Fig. 9. The measured component consists of two symmetrical parts, the photograph of one half of the component is shown in Fig. 10a ($\alpha = 0.5$) and 10b (rectangular shape). The lower and upper values of the radius are here respectively equal to 1 mm and 10 mm and the lengths of the two parts of the component are both equal to 10 mm (total length of the component is 20 mm). The load that end the component is a rigid walled cavity of radius 6.6 mm and depth 9 mm.

Fig. 11a and b show respectively the amplitudes (dB) and phases (rad) of the pressure transfer function between the input of the D–C component and the bottom (the end) of the cavity, both as function of the frequency (logarithmic scale) in the interval (100 Hz, 3000 Hz). In each figure the gray dashed line and the gray full line represent the analytical results, respectively for the rectangular component and for $\alpha = 0.5$, the black dashed line and the black full line represent the experimental results for the same shapes respectively and the numerical results (the '×' marks for

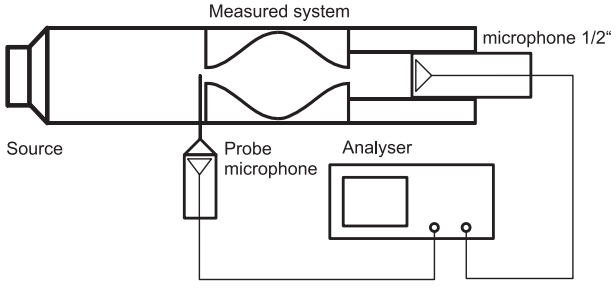

Fig. 9. Experimental set-up for the pressure transfer function measurement.

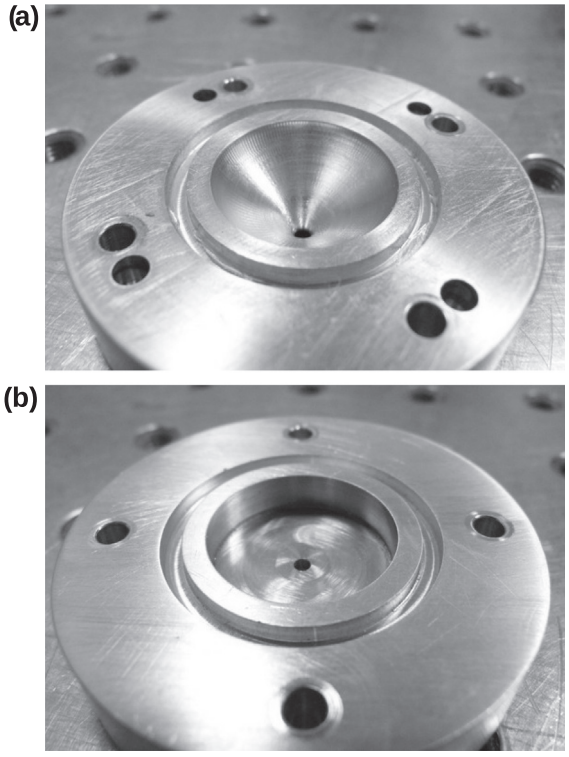

Fig. 10. Photograph of one half of the experimental components before assembly: (a) $\alpha = 0.5$, (b) rectangular shape.

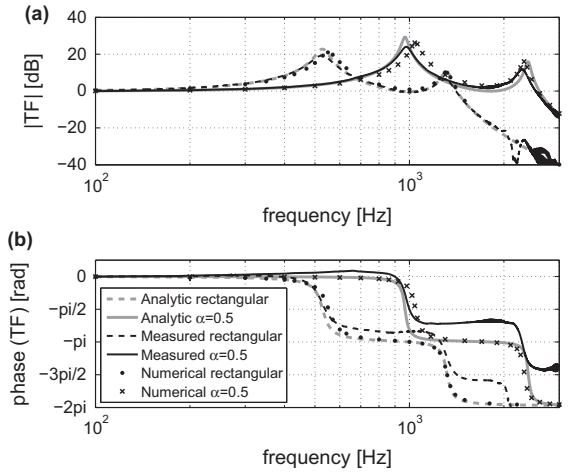

Fig. 11. (a) Amplitude (dB) and (b) phase (rad) of the experimental (black full lines for $\alpha = 0.5$ and black dashed lines for rectangular shape), analytical (gray full lines for $\alpha = 0.5$ and gray dashed lines for rectangular shape) and numerical (black points for $\alpha = 0.5$ and '×' marks for rectangular shape) pressure transfer function of the D–C component as function of the frequency (logarithmic scale) respectively in the interval (100 Hz, 3 kHz).

$\alpha = 0.5$ and the '+' marks for the rectangular shape) are presented as well. The curves show very good agreement between the analytical and the experimental results, thereby supporting analytical results, namely the fact that the value of the parameter could have a decisive influence on the resonant frequency, without modifying significantly the Q-factor and the amplitude of the resonances. The discrepancies between the experimental and the analytical results could be explained by the limited precision in the fabrication and by the approximation made in the analytical calculations including the underestimating of the damping on the geometrical

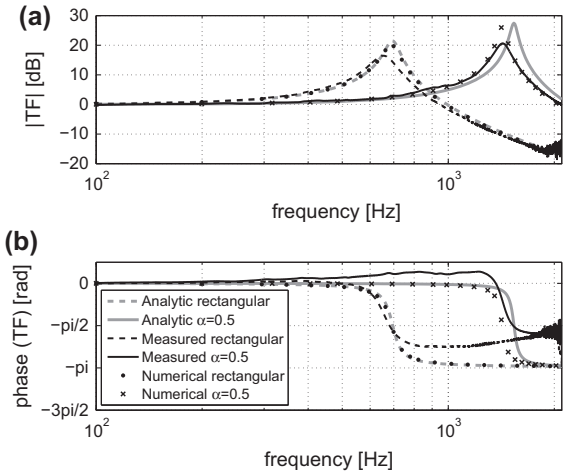

Fig. 12. (a) Amplitude (dB) and (b) phase (rad) of the experimental (black full lines for $\alpha = 0.5$ and black dashed lines for rectangular shape), analytical (gray full lines for $\alpha = 0.5$ and gray dashed lines for rectangular shape) and numerical (black points for $\alpha = 0.5$ and '×' marks for rectangular shape) pressure transfer function of the C–D component as function of the frequency (logarithmic scale) respectively in the interval (100 Hz, 2.1 kHz).

discontinuities at the input and at the output of the component. The discrepancies between the numerical and the analytical results could be explained by the fact that the geometrical discontinuity at the input of the component is not taken into account in the numerical model, while being approximated by an added mass (which leads to lower resonance frequency) in the analytical model.

Fig. 12a and b show respectively the amplitudes (dB) and phases (rad) of the pressure transfer function between the input and the end of the C–D component (symmetric hour-glass shape), both as function of the frequency (logarithmic scale) in the interval (100 Hz, 2100 Hz). This time the 1/2 in. microphone (see Fig. 9) has been pushed into the cavity so that the microphone membrane forms the end of the C–D component which, for simplicity, is assumed to be rigid and isothermal. As in the previous case (Fig. 11) in each figure the gray dashed line and the gray full line represent the analytical results, respectively for the rectangular component and for $\alpha = 0.5$, the black dashed line and the black full line represent the experimental results for the same shapes respectively and the numerical results (the '×' marks for $\alpha = 0.5$ and the '+' marks for the rectangular shape) are presented as well. Apart from the discrepancies which are similar to the ones observed in Fig. 11, the comparison shows that the numerical result for $\alpha = 0.5$ estimates better the position of the resonance frequency than the analytical one. This can be explained by the fact that one of the assumptions made in the analytical solution, the uniformity of the acoustic pressure on the cross-section of the component, is no longer valid when the input diameter is so large (thus showing the limitation of the analytical method) and also by the fact that for C–D component the experimental result is more influenced by the uncertainty of the position of the input of the probe microphone at the input of the component.

4. Conclusion

In conclusion, the results obtained show the potentialities of both the unique analytical representation of small components whose the diameter depends on the axial coordinate (the shape being governed by only three parameters in each element), which is well adapted when designing such components for given applications, and the decisive influence of the value of these parameters on the behavior of these small acoustic components (which could be of interest in devices made up of these components when matching a given pattern is hoped).

Acknowledgements

The authors are very grateful to the reviewer for their detailed comments which helped them to improve the paper.

Appendix A. The tapered tube [11]

The appropriate wave equation is the one-dimensional Webster's horn equation which governs the pressure variation, assumed herein to be driven by a uniform acoustic pressure $p(0)$ at the input $x = 0$ of the horn. It is expressed as follows (∂_x standing for $\partial/\partial x$):

$$\left[\partial_{xx}^2 + \sigma(x)\partial_x + k_0^2 f(x)\right] p(x) = 0, \tag{A.1}$$

where

$$\sigma(x) = \partial_x G(x)/G(x), \tag{A.2}$$

$G(x)$ depending on the cross-sectional area of the horn and on the series impedance per unit length (related to the viscous boundary layer effects), and where

$$k^2(x) = k_0^2 f(x) \tag{A.3}$$

is the complex wavenumber with $k_0^2 = \omega/c_0$, the thermo-viscous effects being covered by the function $f(x)$, which accounts for the angular frequency ω of the field and the properties of the fluid, namely the compressibility χ_0 and the density ρ_0 through the adiabatic speed of sound c_0, the heat capacity at constant pressure per unit of mass C_P, the specific heat ratio γ, the shear viscosity coefficient μ, and the thermal conduction coefficient λ_h.

Given the following change of variable

$$x \to \xi = \int_0^x [G(0)/G(x')]\,\mathrm{d}x', \tag{A.4}$$

the first spatial derivative (Eq. (A.1)) can readily be removed, and what results is:

$$\left[\partial_{\xi\xi}^2 + k_0^2 \phi(\xi)\right] p(\xi) = 0, \tag{A.5}$$

where

$$\phi(\xi) = G_0^2(x) f(x), \tag{A.6}$$

with $G_0(x) = G(x)/G(0)$. Note that the change of variable (Eq. (A.4)) can be written herein as:

$$\xi(w) = \varepsilon \frac{L}{U} \int_0^w \frac{F_v(0)R^2(0)}{F_v(t)R^2(t)} \cos(\theta_0 t^\alpha)\,\mathrm{d}t, \tag{A.7}$$

where $\varepsilon = +1$ when using Eqs. (4) and (5) and $\varepsilon = -1$ when using Eqs. (6) and (7) and where F_v accounts for the effects of the viscous boundary layer [11]. This last expression is readily derived from using the expression of $G(x) = F_v(x)S(x)$ [11, Eq. (6)] and the expressions (4)–(7) along with Eq. (1) for the integration variable x', leading to $\mathrm{d}x' = \varepsilon \frac{L}{U} \cos(\theta_0 t^\alpha)\,\mathrm{d}t$. The analytical solution of the Helmholtz Eq. (A.5) can be formally expressed from using the following equivalent couple of equations

$$\begin{cases} \partial_\xi q(\xi) + k_0^2\ \phi(\xi)\ p(\xi) = 0, \\ \partial_\xi p(\xi) = q(\xi). \end{cases} \tag{A.8}$$

The quantity q may be thought of as proportional to the complex amplitude of the time rate at which volume of fluid is being added to the medium per unit of time through the unit surface, namely the volume velocity field $U(x)$.

By integration over the interval $(0, \xi)$, and integrating the second equation by part, this couple of equation leads readily to the Volterra integral equations:

$$\begin{cases} \partial_\xi p(\xi) = \partial_\xi p(0) - k_0^2 \int_0^\xi \phi(\zeta)\, p(\zeta)\, \mathrm{d}\zeta, \\ p(\xi) = p(0) + \partial_\xi p(0)\, \xi - k_0^2 \int_0^\xi (\xi - \zeta)\, \phi(\zeta)\, p(\zeta)\, \mathrm{d}\zeta. \end{cases} \tag{A.9}$$

The order of magnitude of the last term in the right hand side of this equation is given by the square of the ratio of the length of the horn and the wavelength, i.e. $[k_0 \ell/(2\pi)]^2$. Then, assuming the hypotheses presented above in Section 3.1, this term is assumed to be much lower than the zero order pressure linear profile (denoted p_0)

$$p_0(\xi) = p(0) + \partial_\xi p(0)\, \xi. \tag{A.10}$$

It follows that the Born approximation of Eq. (A.9) leads to the first order solution

$$\begin{aligned} p_1(\xi) &= p(0) + \partial_\xi p(0)\, \xi - k_0^2 \int_0^\xi (\xi - \zeta)\, \phi(\zeta) p_0(\zeta)\, \mathrm{d}\zeta, \\ \partial_\xi p_1(\xi) &= \partial_\xi p(0) - k_0^2 \int_0^\xi \phi(\zeta) p_0(\zeta)\, \mathrm{d}\zeta. \end{aligned} \tag{A.11}$$

Then, from this equation the transfer matrix of the acoustic element is obtained easily.

References

[1] Zwikker C, Kosten CW. Sound absorbing materials. Amsterdam: Elsevier; 1949.
[2] Škvor Z. Vibrating systems and their equivalent circuits. Amsterdam: Elsevier; 1991.
[3] Bruneau M, Scelo T. (Translator and contributor): Fundamentals of acoustics, ISTE, UK, USA; 2006.
[4] Ortiz S, Kolbrek B, Cobo P, Gonzales LM, De La Colina C. Point source loudspeaker design: advances on the inverse horn approach. J Audio Eng Soc 2014;62:345–54.
[5] Grinnip RS. Advanced simulation of condenser microphone capsule. AES 117th convention. San Francisco; 2004.
[6] Lesniewski P. Discrete component equivalent circuit for Webster's horns. Appl Acoust 1995;44:117–24.
[7] Rund F. Modeling of acoustic waveguides using electro-acoustic analogy: application to the human ear canal. In: Proceedings of Internoise 2004. Prague: Czech Acoustical Society; 2004. p. 793.
[8] Rodrigues D, Guianvarc'h C, Durocher J-N, Bruneau M, Bruneau A-M. A method to measure and interpret input impedance of small acoustic components. J Sound Vib 2008;315:890–910.
[9] Honzík P, Škvor Z, Durand S, Bruneau M. Electrostatic transducer with square membrane and non-planar back plate: simplified model. Acta Acust United Acust 2009;95:671–86.
[10] Bravo A, Barham R, Ruiz M, Lopez JM, De Arcas G, Alonso J. A new 3D finite element model of the IEC 60318-1 artificial ear: II. Experimental and numerical validation. Metrologia 2012;49:785–802.
[11] Honzík P, Durand S, Joly N, Bruneau M. On the acoustic transfer function of slowly tapered small horns filled with thermo-viscous fluid. Acta Acust United Acust 2013;99:694–702.
[12] Schuhmacher A, Rasmussen KB. Modelling of horn-type loudspeakers for outdoor sound reinforcement systems. Appl Acoust 1999;56:25–37.
[13] Joly N. Finite element modeling of thermoviscous acoustics on adapted anisotropic meshes: implementation of the particle velocity and temperature variation. Acta Acust United Acust 2010;96:102–14.
[14] Joly N, Bruneau M, Bossart R. Coupled equations for particle velocity and temperature variation as the fundamental formulation of linear acoustics in thermo-viscous fluids at rest. Acta Acust United Acust 2006;92:202–9.
[15] Honzík P, Joly N, Durand S, Rodrigues D, Durocher J-N, Bruneau M. Finite element modelling of acoustic field inside small components: application to an annular slit terminated by an aperture in an infinite screen. Metrologia 2012;49:32–40.